Archaeological Prospection
Archaeol. Prospect. **13**, 75–90 (2006)
Published online 13 October 2005 in Wiley InterScience (www.interscience.wiley.com). DOI: 10.1002/arp.271

Contribution of Multiplexed Electrical Resistance and Magnetic Techniques to the Archaeological Investigations at Poros, Greece

N. G. PAPADOPOULOS,[1,2]* A. SARRIS,[1] E. KOKKINOU,[1] B. WELLS,[3] A. PENTTINEN,[3] E. SAVINI,[3] G. N. TSOKAS[2] AND P. TSOURLOS[2]

[1] *Laboratory of Geophysical–Satellite Remote Sensing and Archaeo-environment, Institute for Mediterranean Studies, Foundation for Research and Technology—Hellas, P.O. Box 119, Rethymnon, 74100, Crete, Greece*
[2] *Laboratory of Applied Geophysics, School of Geology, Aristotle University of Thessaloniki, 54124, Thessaloniki, Greece*
[3] *Swedish School at Athens, Mitseon 9, Athens 11742, Greece*

ABSTRACT The Sanctuary of Poseidon at Kalaureia is located on the island of Poros in the Saronic Gulf in Greece. Two Swedish archaeologists first carried out excavations at the site in 1894; in 1997 investigations were resumed by the Swedish Institute at Athens. Although there are traces of occupancy in the area by the early Bronze Age, the results so far attest to some activity in the very late Bronze Age (ca. 1100 BC); with a considerable proportion of the remains dating from the eighth century BC and the visible remains dating to the sixth to second centuries BC.

A geophysical investigation was conducted at the site using both electrical resistance techniques and magnetic methods. A small area of 20 × 15 m at the southeast section of the site was surveyed with high-resolution multiplexed electrical resistance techniques in order to maximize the information content of the subsurface remains in both horizontal and vertical extent.

The local vertical magnetic gradient of the Earth's magnetic field was measured using a fluxgate gradiometer, and multiplexed electrical resistance techniques were applied in order to map the subsoil resistance at different depths. In addition, the whole area was investigated with a double twin probe configuration.

Emphasis was given to the use of the multiplex electrical resistance technique with different configurations. A small grid to the southeast of the survey area was investigated with a twin probe configuration, recording the subsurface resistance at four increasing depths. Additionally, 0.5 m dipole–dipole and 0.5 m Wenner mapping configurations were performed. The above data were processed using a specifically developed processing package (GPP). The resistance instrument was also programmed in such a way as to conduct parallel resistance tomographies along the x and y directions with a pole–pole array. Copyright © 2005 John Wiley & Sons, Ltd.

Key words: resistance mapping; magnetic gradient; multiplexer; GPP package; resistivity inversion

* Correspondence to: N. G. Papadopoulos, Laboratory of Geophysical–Satellite Remote Sensing and Archaeo-environment, Institute for Mediterranean, Foundation for Research and Technology—Hellas, P.O. Box 119, Rethymnon, 74100, Crete, Greece. E-mail: nikos@ims.forth.gr

Received 8 March 2005
Accepted 29 June 2005

Introduction

The island of Poros lies about 30 nautical miles south of Piraeus in the Saronic Gulf. Poros is actually two islands: Kalaureia and Spheria, separated by a narrow channel. It is on the larger of the two, Kalaureia, that the sanctuary of Poseidon is situated.

The sanctuary lies in the centre of the island, on a saddle between the two hills Vigla and Prophitis Elias, at an altitude of 190 m above sea level. It was first investigated by Samuel Wide and Lennart Kjellberg (1895), but apart from Gabriel Welter's study of the architecture in the 1930s (Welter, 1941), no further fieldwork had been carried out at the site, until the Swedish Institute at Athens was invited to continue excavations in 1996. This work began the following year under the direction of Berit Wells.

Extensive cleaning of the site was needed, as the first excavators had left their spoil heaps by the walls as they were uncovered. Moreover, at the beginning of the twentieth century the area of the sanctuary had been turned into a farmstead, the buildings of which quickly dilapidated after the expropriation of the land in 1978, leaving masses of debris from the ruined buildings.

The sanctuary as we know it today consists of the temple area within a peribolos (defensive wall) in the northeast and to the southwest an open area, around which lie five buildings: a possible entrance building in the far southwest, two stoas or porticoes in the northwest, and one stoa and a complex with dining rooms and courtyards in the southeast. Excavation has so far focused on the two latter buildings, which are designated Buildings C and D. They can both be dated to the end of the fourth century BC. Typically, it is in this direction that the sanctuary always expanded—and could expand owing to the lie of the land—represented by at least three stages of deliberate terracing from the seventh to the fourth century BC (Wells *et al.*, 2003).

In 2003 a comprehensive programme was initiated with the aim of studying occupation activity in the sanctuary, the physical environment within it and the sanctuary in a wider archaeological landscape. It was also decided to investigate the unexcavated areas through remote sensing in order, hopefully, to learn more about the layout of the sanctuary and of its total extent (Wells *et al.*, 2005).

In the spring of 2004 a geophysical campaign was conducted at the site by the Laboratory of Geophysical–Satellite Remote Sensing and Archaeoenvironment of the Institute for Mediterranean Studies/Foundation of Research and Technology at Hellas (FORTH). The goal of the research was to indicate where possible locations of archaeological interest may exist. An area of about 3000 m^2 was covered using both electrical resistance techniques and magnetic methods. The area of interest was divided into three regions, namely areas A, B and C (Figure 1). Additionally, a 20×15 m grid (area C4), at the southeast section of the site, was used to investigate different earth resistance techniques and methods.

Methods

The areas of interest were surveyed using both magnetic and electrical resistance methods. The Geoscan FM36 fluxgate gradiometer was used to measure the vertical magnetic gradient of the local magnetic field with a step interval of 0.5 m along both x and y axes. The resistance measurements were made using the Geoscan RM15 soil resistance meter. The RM15 was used together with the MPX15 multiplexer and the whole area was investigated with a double twin probe configuration. The mobile electrode spacing was set to 0.5 and 1 m respectively, and the step interval was 1 m. In this way, the goal of measuring soil resistance at two different depth layers was accomplished.

A rectangular area of 20×15 m at the southeast section of the archaeological site was covered using the electrical resistance technique. The grid was surveyed along south–north and west–east directions. Different probe configurations were tested in order to evaluate their effectiveness and resolution in the detection of buried archaeological structures. The area was also surveyed with a Geoscan Research FM36 fluxgate gradiometer with a 0.5 m sampling interval.

The resistance measurements were made with the Geoscan Research RM15 soil resistance meter, which was used along with the Multiplexer

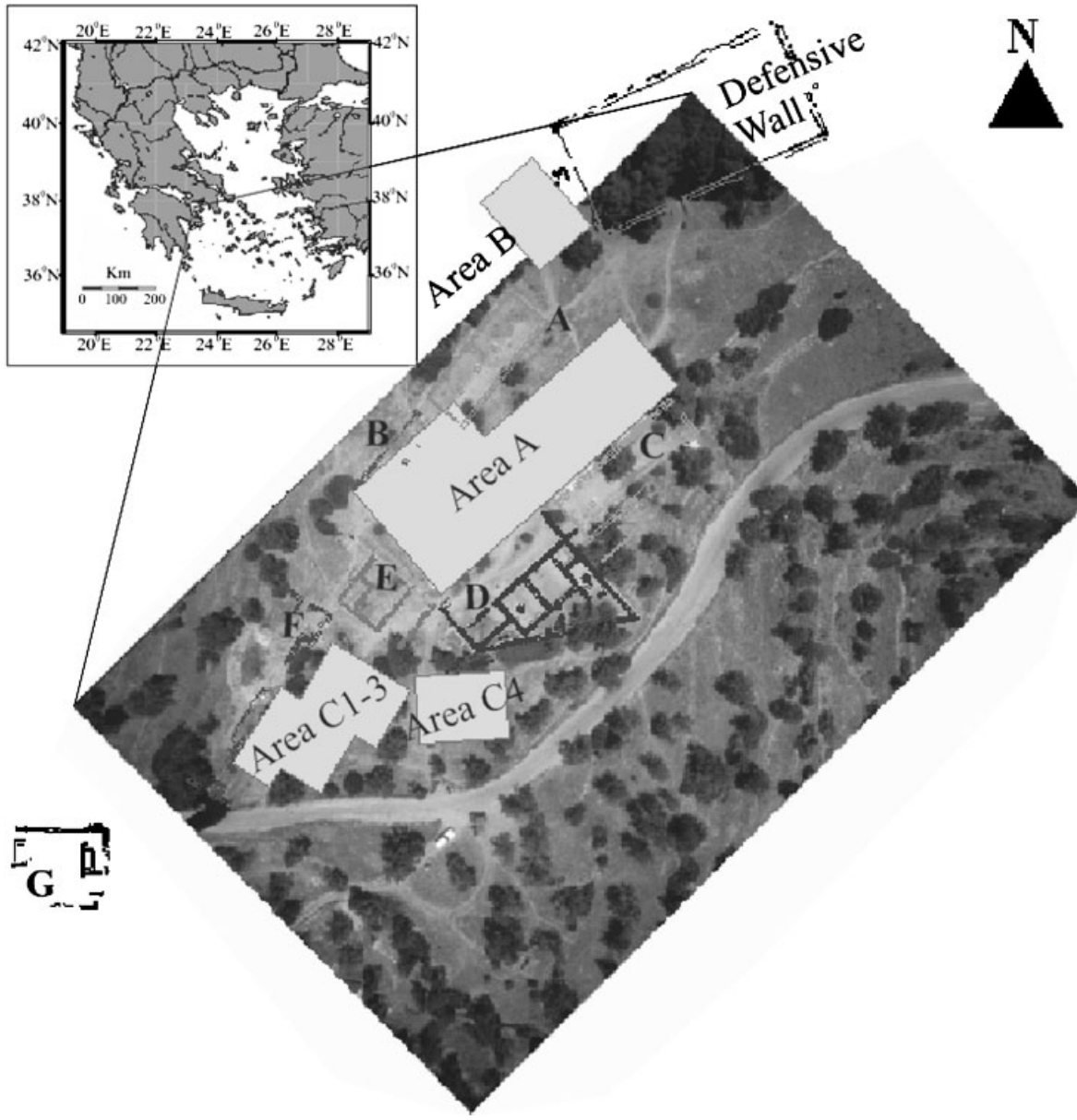

Figure 1. Aerial photograph of the Kalaureia archaeological site where excavated ruins (with their code letters) and the geophysical grids have been superimposed.

MPX15 and the multiprobe frame PA5. The combined use of the multiplexer with the PA5 frame and the RM15 resistance meter offers a wider range of probe arrays such as multiple twin probe, simultaneous measurements of Wenner, dipole–dipole, etc. The instrument also can be modified to store a user defined sequence of configurations.

The RM15–MPX15 system was used to map the subsurface apparent resistance with multiple twin probe configuration at 0.5 m, 1 m, 1.5 m and 2 m separation between the mobile probes (Figure 2A). The sample interval was set to 1 m for the 0.5 m and 1 m twin probe configuration and 0.5 m for the 1.5 m and 2 m mobile electrode spacings. The gradual increase of the distance

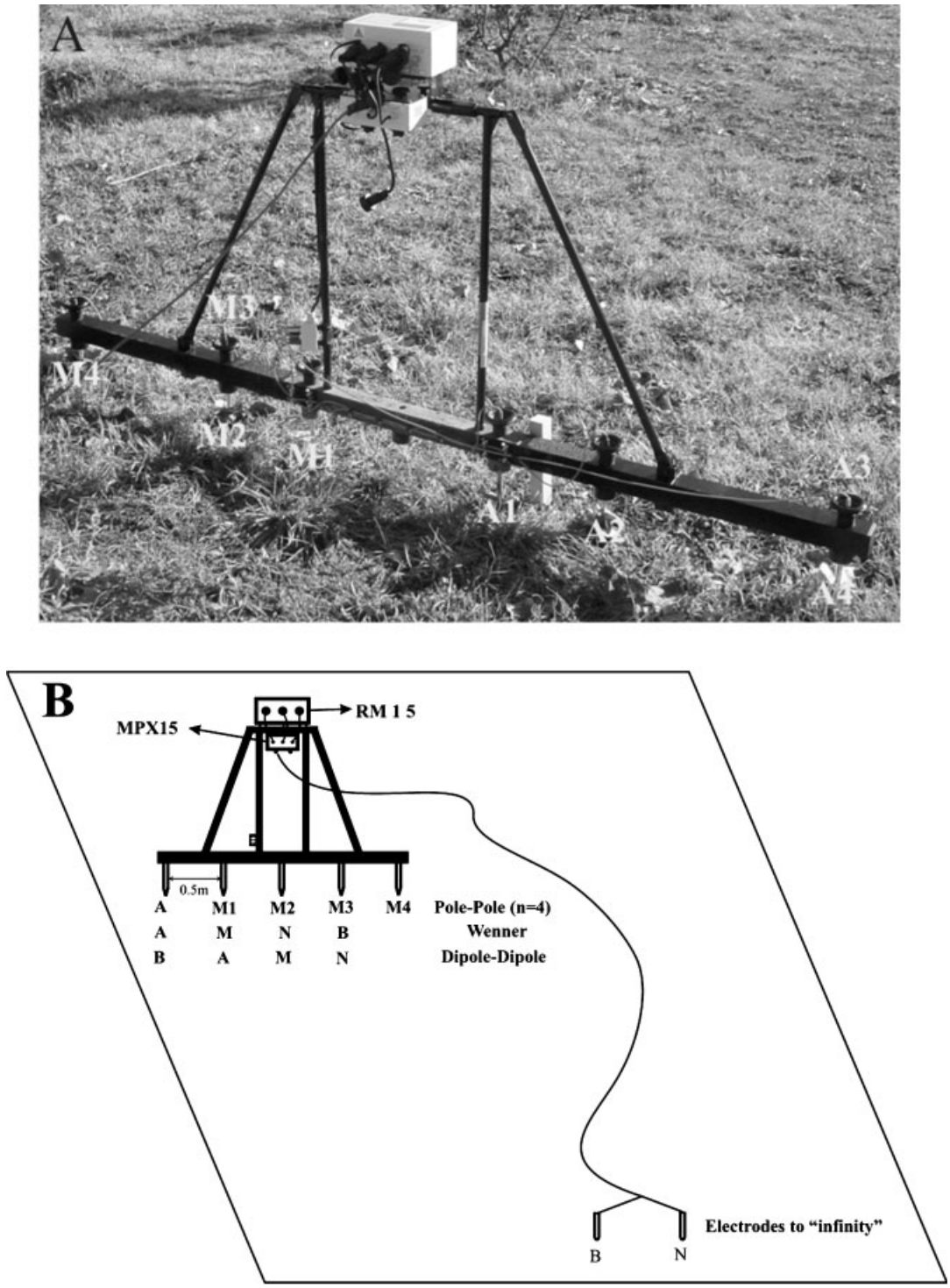

Figure 2. (A) Connection of the RM15 resistance meter with the multiplexer MPX15 and the multiprobe frame PA5 to carry out the multiple four twin probe configuration. (B) Instrument connections used to conduct the subsoil mapping with the Wenner and the dipole–dipole array. Also shown is the electrode configuration so as to conduct the pole–pole parallel tomographies with n_{max} separation equal to 4.

between the mobile probes yields a corresponding increase of the penetration depth. This allows a three-dimensional image of the distribution of apparent resistance in the subsoil to be recorded.

The area was also surveyed with Wenner and dipole–dipole probe array configurations. The separation between the A, B, M and N probes was fixed and equal to 0.5 m, as shown in Figure 2B. The sampling interval was 0.5 m, and the interval between the parallel traverses was set equal to 1 m. Wenner and dipole–dipole probe arrays were chosen as similar configurations are mainly used by electrical tomography techniques.

One additional probe configuration was also deployed, whereby the left electrode was always used as a current electrode (A), and the four other electrodes were used to measure the potential (M1, M2, M3 and M4). The distance between the pair of electrodes A-M1, A-M2, A-M3 and A-M4 was 0.5 m, 1 m, 1.5 m and 2 m correspondingly (Figure 2B). The goal was to gather parallel tomographic resistivity data with the pole–pole array from four increasing depth layers. Tomographic sections parallel to the x axis were conducted by moving the frame along the south–north direction, with a 0.5 m step interval, in a parallel mode, and those parallel to the y axis were conducted by moving the instrument along the west–east direction. In this way 71 tomographic profiles were collected, 31 parallel to the x axis and 40 parallel to the y axis. The distance between the parallel tomgraphies was 0.5 m.

Data processing

Each data set was coded with a unique grid number. Data sets were given the appropriate coordinates according to the position of the adjacent grids and an area code was given for each cluster of grids. Each mosaic of geophysical grids was orthorectified through registration of them to the Hellenic Geodetic Reference System of coordinates (namely HGRS'87), based on the GPS/EDM mapping data.

All data were characterized by a constant shift of the average value within each surveyed grid owing to differences in balancing the instrument and the shifting of the base/reference stations. For this reason, pre-processing of the data was needed in order to create a common base level (zero-mean base line) for all grids. Statistical analysis of both the common rows and the calculation of the average level of adjacent grids were carried out in order to provide a correction factor for each grid. Both the change of coordinates and the correction factors were used to create the mosaic of the grids in each area. In this way, processing of the adjacent grids was conducted simultaneously.

Most data sets were processed with a specific method. Kriging interpolation was used for gridding the data. In some cases, selective despiking techniques were used to isolate the extreme values that masked the anomalies of interest. Selective compression of the dynamic range of values was also used to isolate anomalies close to the background level. A mask file was created to isolate the areas that were not surveyed owing to the existence of thick vegetation, fences, modern structural remains and other surface features.

The above processes with the exception of masking were carried out using the GPP package (Kalokerinos *et al.*, 2004). The GPP package has been developed on a LINUX platform using a GCC compiler, which was then ported using a Borland C compiler in order to be executed in a command (GCC) window in the WINDOWS NT environment. Preprocessing options of the GPP include geometry correction of the grids, evaluation of statistical parameters, mutation of dummy values and shifting of the X and Y coordinates. Main processing includes the application of despiking techniques based to the noise level (estimated by the dynamic range of measurements and the standard deviation from the mean), grid equalization and line equalization to smooth out the data and to avoid stripping effects. Secondary options of the GPP package include resampling of the data by any step in the X and Y directions and exclusion of the dummy values. The GPP package is also able to make a mosaic of grids at any stage of processing (preprocessed and main processed grids). A simple flowchart of the algorithm is shown in Figure 3.

The GPP package is able to deal with a large number of grids within a relatively small amount

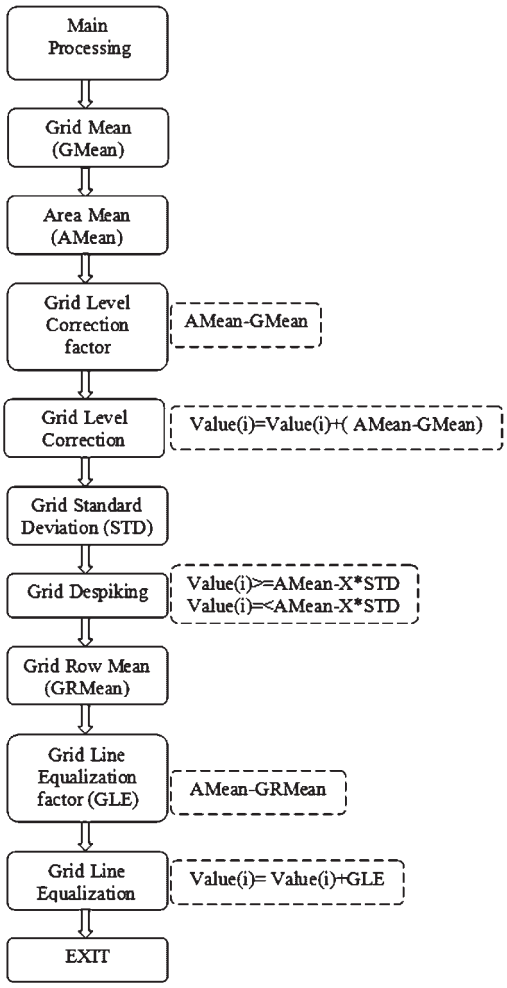

Figure 3. Flowchart diagram of the main functions of the GPP software package.

of time. The processed data are exported in a format appropriate for the Surfer mapping package, where various types of maps of high quality can be created. The software also has been tested with very noisy real data (Kalokerinos *et al.*, 2004) and proved its efficiency and reliability. Recently, it has been adopted by the authors in the main course of processing and interpreting electrical resistance, magnetic and electromagnetic data collected from archaeological sites.

The resistance data collected from area C4 were initially converted to resistivity values by multiplying the resistance measurements with the appropriate geometrical factors. The conversion equation from apparent resistance measurements (R) to apparent resistivity values (ρ) for the dipole–dipole array is given by $\rho = 6\pi Ra$ and for the Wenner array by $\rho = 2\pi Ra$, where a is the distance between the electrodes. The value of a for both arrays was fixed and equal to 0.5 m. For the twin probe configuration the conversion formula $\rho = 2\pi R\,ab/(a+b)$ was used, where a is the distance between the mobile electrodes (A and M) and b the distance between the remote electrodes (B and N), which are considered to be at 'infinity'. The a parameter had values equal to 0.5 m, 1 m, 1.5 m and 2 m, and b was measured to be 1.6 m for the south–north survey and 1.7 m for the west–east survey. Afterwards the transformed resistivity data were processed using the methods mentioned above.

The tomographic data were inverted using a smoothness constrained two-dimensional non-linear algorithm. The governing differential equation for the geolectrical problem is solved numerically using the finite element method (FEM) (Tsourlos, 1995). The subsurface is considered as a set of individual blocks, which are called parameters, and they are allowed to vary their resistivities independently. The aim is to calculate a subsurface estimate of the apparent resistivity for which the difference between the observed and the calculated data, which are calculated with the FEM method, is minimized. As the resistivity problem is a non-linear problem, this procedure has to be iterative. In every iteration an improved resistivity estimate is sought and eventually the procedure continues until certain criteria are met (e.g. more or less stable RMS).

The resistivity estimate at the $k+1$ iteration is given by the formula (Constable *et al.*, 1987; Sasaki, 1989, 1992; deGroot-Hedlin and Constable, 1990; Tsourlos, 1995)

$$x_{k+1} = x_k + \left[\left(\mathbf{J}_k^T\mathbf{J}_k + m_k\mathbf{C}^T\mathbf{C}\right)^{-1}\mathbf{J}_k^T(y - F(x_k)\right] \quad (1)$$

where $\boldsymbol{y}$ is the measured data vector, $\mathbf{J}_k$ is the Jacobian of the x_k resistivity distribution, $F(x_k)$ is the forward modelling operator, $\mathbf{C}$ is the smoothness matrix and m_k is the Lagrangian multiplier. The superscript T in Equation (1) indicates the transpose of the relevant matrix.

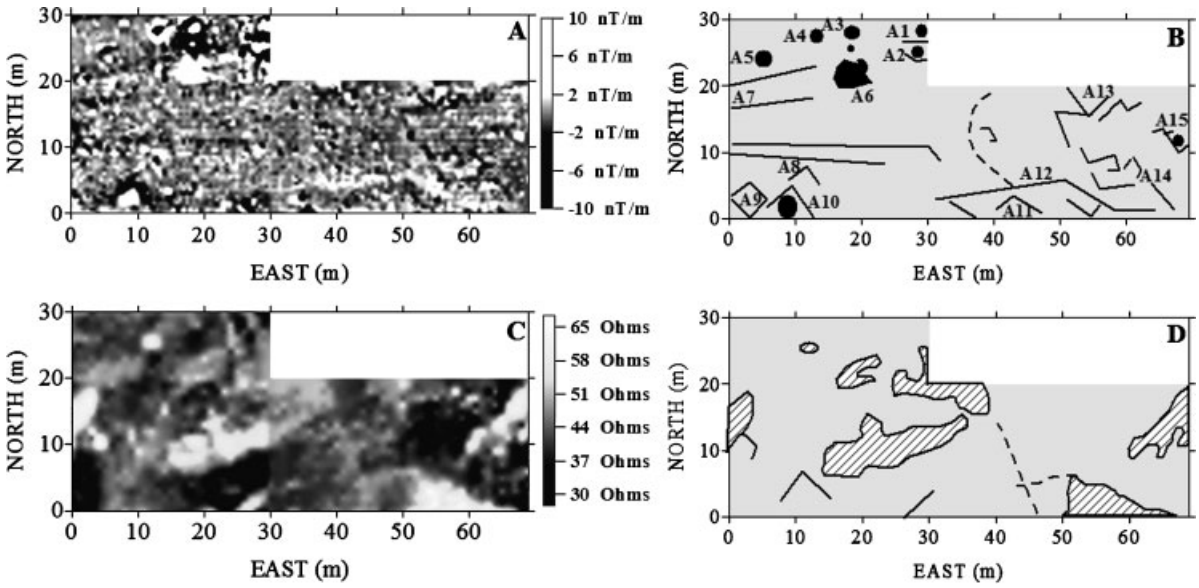

Figure 4. (A) Vertical magnetic gradient map from Area A of the archaeological site. (B) Diagrammatic interpretation of the magnetic anomalies. (C) Resistance map from Area A of the site. (D) Diagrammatic interpretation of the resistance anomalies.

Results

Area A

Area A was an open area, clear of vegetation. The magnetic map and its diagrammatic interpretation indicate a number of linear anomalies at the west, centre and east of the area, which are probably caused by buried remains (Figure 4A and B).

Anomalies A1 and A2 are located at the north side of the area, and anomalies A3, A4 and A5 are located above the position of column bases, most of which are found *in situ*. The diffuse response close to anomaly A2 originates from the existence of a pile of stones and a tree located just to the south of A2.

A few linear trends (anomalies A7 and A8) are also indicated towards the western part of the map, projecting to the east or northeast. As these anomalies are not present in the soil resistance map (Figure 4C and D) it is unclear if they constitute traces of roads/paths leading towards the sanctuary to the east.

Further to the southwest there is strong evidence for the presence of architectural remains (A9 and A10). The outline of the anomalies shows a general orientation along a NW–SE direction. Anomaly A10 seems to enclose a strong magnetic feature to the south, probably related to a hearth.

A few more linear anomalies are shown to the east and southeast section of the map and their orientation is similar to that of A9 and A10. Anomaly A12 extends for more than 10 m along a SE–NW direction, turning to a slightly opposed direction to the west for more than 20 m. It is possible that the above features are also related to structural remains.

A different picture is presented by the soil resistance measurements in the same area (Figure 4C and D). Areas of high electrical resistance may represent outcrops of the shallow depth bedrock, suggesting that there is a thin soil layer remaining to the site, which in combination with the type of structural materials used in the settlement has created a weak correlation between the magnetic and soil resistance anomalies.

The above anomalies indicate that the eastern section of the site contains a number of architectural relics that are probably adjacent to building complexes A and C. Anomalies A8–A10 also may represent a continuation of building D, and the

linear anomalies that are suggested in the central western section of the geophysical maps could originate from traces of paths leading from building E towards the sanctuary or the rest complexes to the northern side (complexes A and B).

Area B

Area B extends southwest of the temple, at an elevation difference of more than 2.5–3 m above the terrain where the sanctuary lies. Magnetic signals (Figure 5) were much more informative than soil resistance data, although the presence of metal stakes in the area of interest (x, $y = 2.5$E, 16N and x, $y = 11.5$E, 8.5N, corresponding to anomalies B1 and B3) have obscured a large part of the survey area. Of major importance are the linear features B5, B6, B7, B8 and B9, which probably indicate the existence of architectural remains. More specifically, anomalies B6 and B7 may designate the continuation of wall remnants which are evident at the eastern scarp of the terrace towards the sanctuary. On the other hand, the different orientation of anomalies B8, B9, B10 and B11 may suggest the existence of structural remains belonging to a different occupation phase. Finally, the dipole nature of B2 and B4 may indicate the existence of metal fragments (Figure 5).

Area C1–3

The magnetic data exhibit a number of features extending mainly towards the south and east parts of the region C1–3 (Figure 6A and B). A few linear anomalies are shown to project in a south to north direction, probably representing traces of paths leading to Area A (towards complex E). Most important, however, is the existence of a number of rectangular features, possibly related to architectural structures existing at the central south and eastern section of Area C1–3. These features (anomalies C5, C6, C7, C8 and C9) show an orientation towards the NW–SE and have approximate dimensions of 3×3 m. The outline of anomaly C10 is rather vague owing to the halo created by anomaly C11 related to a tree in the vicinity. However, it is possible that it consists of two compartments on a similar orientation to the above anomalies (C7, C8 and C9). A less informative picture is suggested by the soil resistance measurements taken in area C1–3. A couple of linear/curvilinear anomalies are shown in close correlation with the magnetic anomalies C2, C3, C6 and C10 (Figure 6C).

Area C4

Wenner and dipole–dipole resistivity mapping

The most significant feature that appears at the eastern part of the area ($x = 13$–18E, $y = 4$–15N) in both datasets (W–E and S–N) of the dipole–dipole and the Wenner resistivity maps (Figure 7) is a rectangular shaped anomaly, probably related to building remains, which seems to be divided into three main compartments aligned along a S–N direction. The central part of the anomaly exhibits high values of resistivity, and the northern and southern parts show a more conductive signal. Furthermore, the linear anomaly at $x = 6$E is delineated by both methods, and in the central part of the region ($x = 6$–13E, $y = 9$–11N) another rectangular structure is suggested. It is worth noting that the geophysical survey along west–east direction indicates the continuation of the rectangular building anomaly to the south.

The maps produced by the dipole–dipole and the Wenner resistivity methods are in a very good agreement as far as the detected building at the eastern part of the area. There are also a number of other linear structures that seem to be in good correlation with each other, and some minor anomalies at the central lower left region are shown mainly in the dipole–dipole measurements. Generally the dipole–dipole mapping technique produced images that were superior compared with the Wenner technique, especially in terms of the outline of the structure and its internal compartments.

Multiplexed twin probe configuration

The apparent resistivity maps for the four different depth layers along both directions are presented in Figure 8, and a comparison of the diagrammatic representation of the potential resistivity targets for each method along the two different directions of the survey is shown in Figure 9.

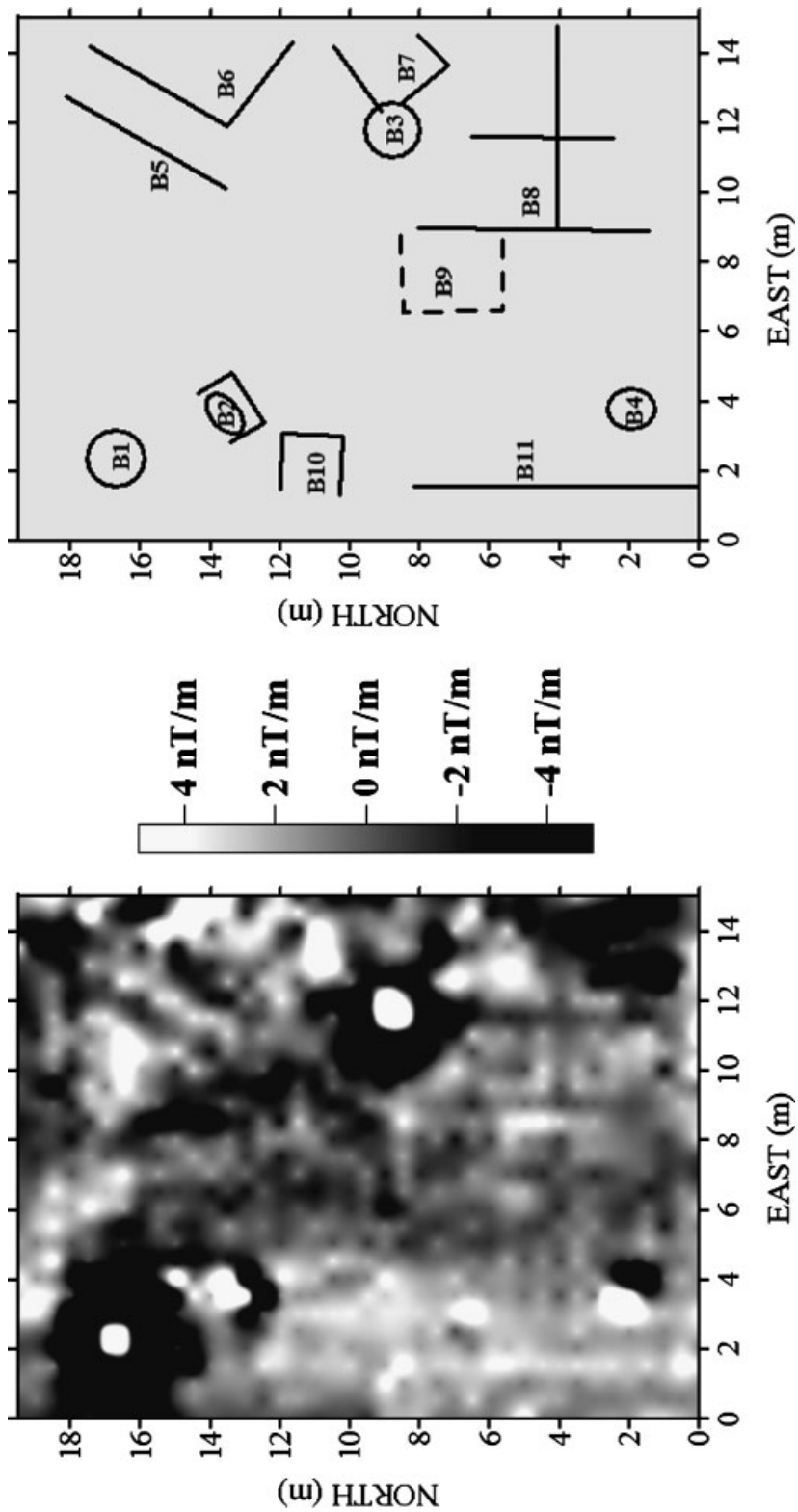

Figure 5. (A) Magnetic map from Area B of the Poros archaeological site. (B) Diagrammatic interpretation of the magnetic anomalies.

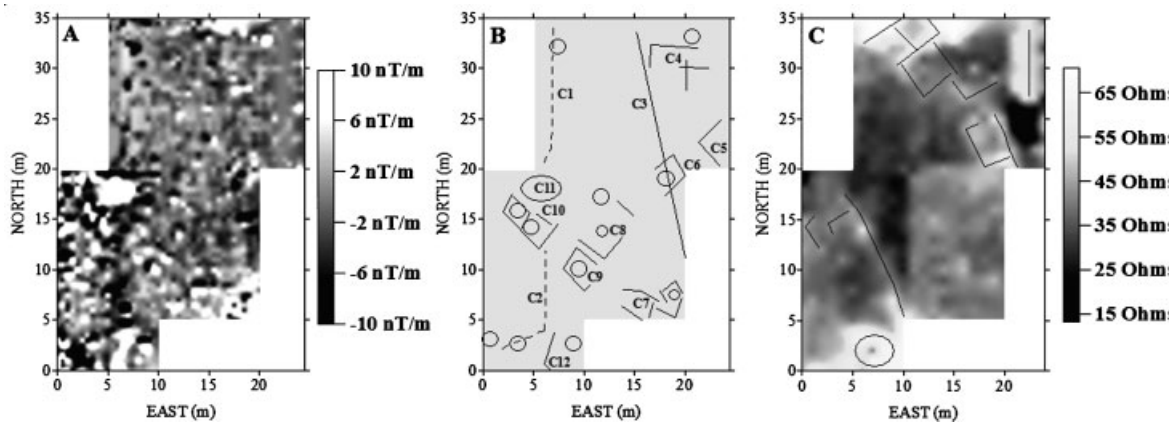

Figure 6. (A) Magnetic map from Area C1–3 of the archaeological site. (B) Diagrammatic interpretation of the magnetic anomalies. (C) Resistance map from Area C1–3 on which the diagrammatic interpretation has been superimposed.

The diagrammatic interpretation maps for the twin probe arrays along the two survey directions are almost identical. The outline of the buried structure at the east section of the area and the linear anomaly along $x = 6$E are clearly delineated, although it is not possible to define any internal details within the eastern complex. Another rectangular structure is also suggested at the northern central part of the grid ($x = 8$–12E, $y = 9$–12N). According to both twin probe and Wenner array data (along the N–S direction), this anomaly seems to constitute part of a larger circular feature extending in the central part of area C4.

The soil resistivity depth slices can give an indication about the depth extent of the buildings remains at the east side of the area. These data suggest that the remains extend up to the third depth slice, indicating a depth of no more than 1.5 m below the surface. On the other hand, the central north anomaly (located to the northwest of the former one) seems to be located at a more shallow depth.

Two-dimensional resistivity inversion

The resistivity tomographies were processed using the 2DINVS software, which is used for the two-dimensional inversion of surface resistivity data, performing a smoothing constrained (Occam's) inversion, and it is based on a 2.5 dimensional finite element forward scheme (Tsourlos, 1995). The 2DINVS software can deal with a wide spectrum of electrode arrays. The Jacobian matrix (i.e. the changes of the apparent resistivity data with respect to resistivity parameters) in the 2DINVS software is calculated using the adjoint equation approach (McGillivray and Oldenburg, 1990). There is also an option for quasi-Newton update of the Jacobian matrix in order to speed up the inversion, and the parameters of the problem can be decided either automatically or by the user, including the adjustment of the model smoothness (Tsourlos, 1995).

Several values of the Lagrangian multiplier were tested and finally a value of 0.2 was chosen. The Lagrangian multiplier is one way to control the smoothness of the inverted model. In general, the larger the value of the Lagrangian multiplier, the smoother the model that will be produced. The maximum number of iterations was set equal to ten. All the inversions completed the ten iterations except for one, which completed eight. It took about 30 min to invert all 71 resistivity tomographies. The mean root square error of the tomographies parallel to the x axis was 2.977% and the one corresponding to the tomographies parallel to y axis reached a value of 3.474%.

The results from the inversion of the tomographies parallel to the x axis, parallel to the y axis and parallel to both of the axes were combined and presented as horizontal depth slices, so they can be compared directly with the apparent resistivity maps (Figure 10).

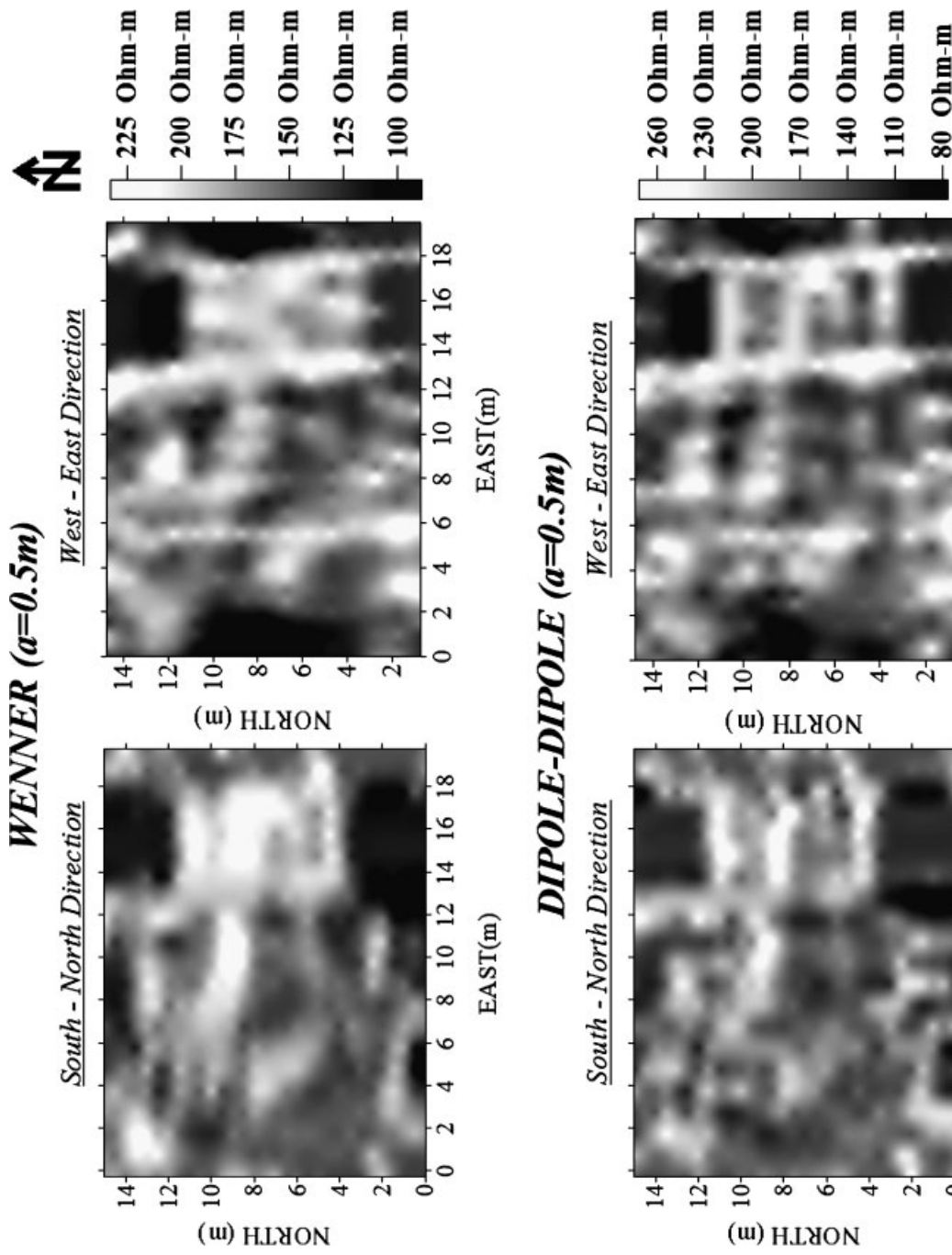

Figure 7. Greyscale image of apparent resistivity maps of the surveyed area with the Wenner and the dipole–dipole array, along south–north direction and west–east directions (*a* is the electrode spacing).

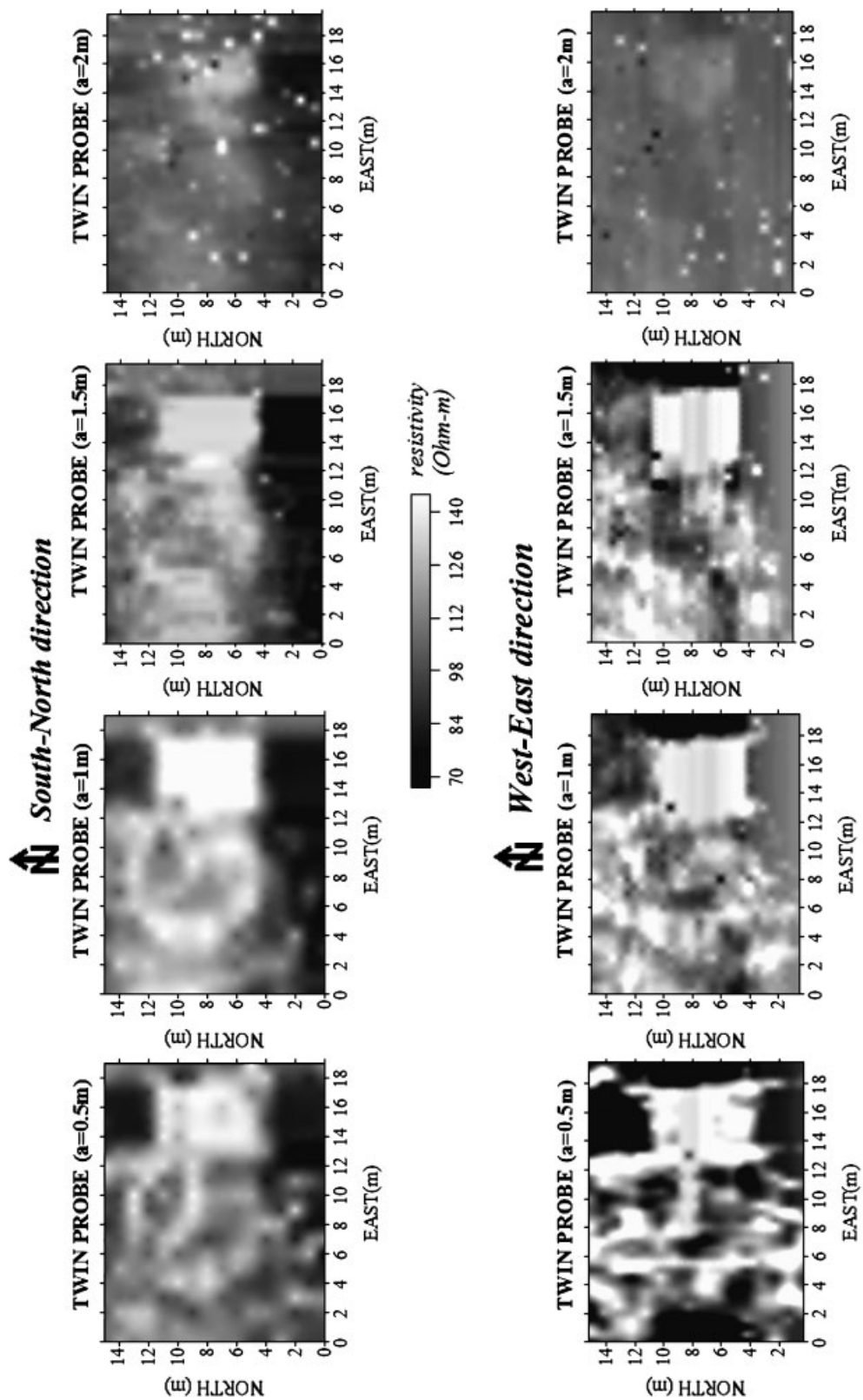

Figure 8. Three-dimensional apparent resistivity distribution of the subsurface by using the four twin probe multiplexed configurations along south–north and west–east directions (*a* is the electrode spacing).

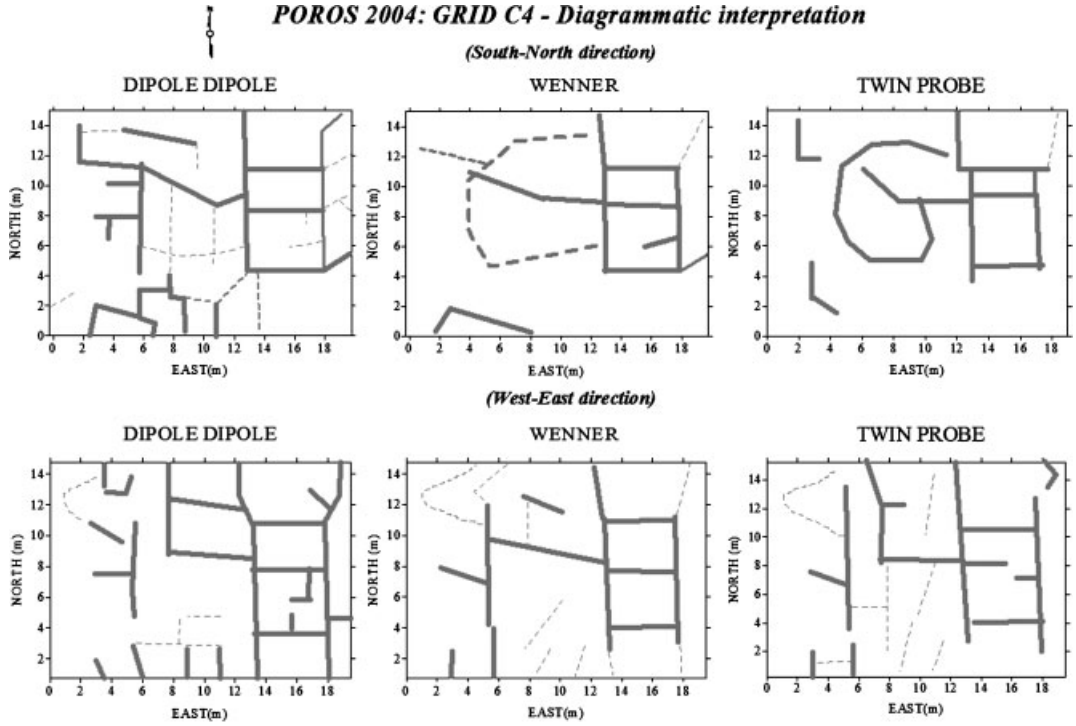

Figure 9. Diagrammatic interpretation of the resistivity anomalies detected in grid C4 with the dipole–dipole, Wenner and twin probe methods along south–north and west–east directions.

The first depth slice (0–0.25 m) coincides with the topsoil consisting of a very small number of buried features. Within the depth range of 0.25–0.5 m, the high resistivity values related to structural details at the east side of the grid become evident. In addition to the above, a number of internal details indicating various compartments of the sections of the building complex are resolved in the inversion images. In the depth slices of 0.5–0.75 m the two-dimensional x direction inversions mainly enhance structures extending parallel to the y axis. The opposite appears in the case of the two-dimensional y direction inversions. A much more synthetic image of the extent of the structural remains at the specific depth range is indicated by the combination of the inversions along both x and y directions.

Magnetic survey

The Geoscan Research fluxgate gradiometer was used to survey the area with a 0.5 m sampling interval. The original dynamic range (-80 to $+60\,\mathrm{nT\,m^{-1}}$) of the vertical magnetic gradient measurements was compressed by removing the extreme high and low magnetic values (Figure 11). Comparing the magnetic map with any of the previous resistivity maps it becomes obvious that the recorded magnetic measurements lack the wealth of information compared with the resistivity data. With the exception of just a few anomalies at the southwest section of the grid ($x = 0$–5E, $y = 2$–6N) and the central east section of it ($x = 13$–15E, $y = 5$–7N), which can be related to structural remains, all the remaining signals show a much more fragmentary image of the subsurface features, lacking any significant geometry. It is possible that increased noise levels have affected the magnetic measurements, mainly due to the fact that the specific grid is located close to the entrance of the site, which is the locus of different modern activities (cemented posts, fences, displaced construction blocks from various parts of the archaeological site, collection and burning activities of the vegetation, etc.).

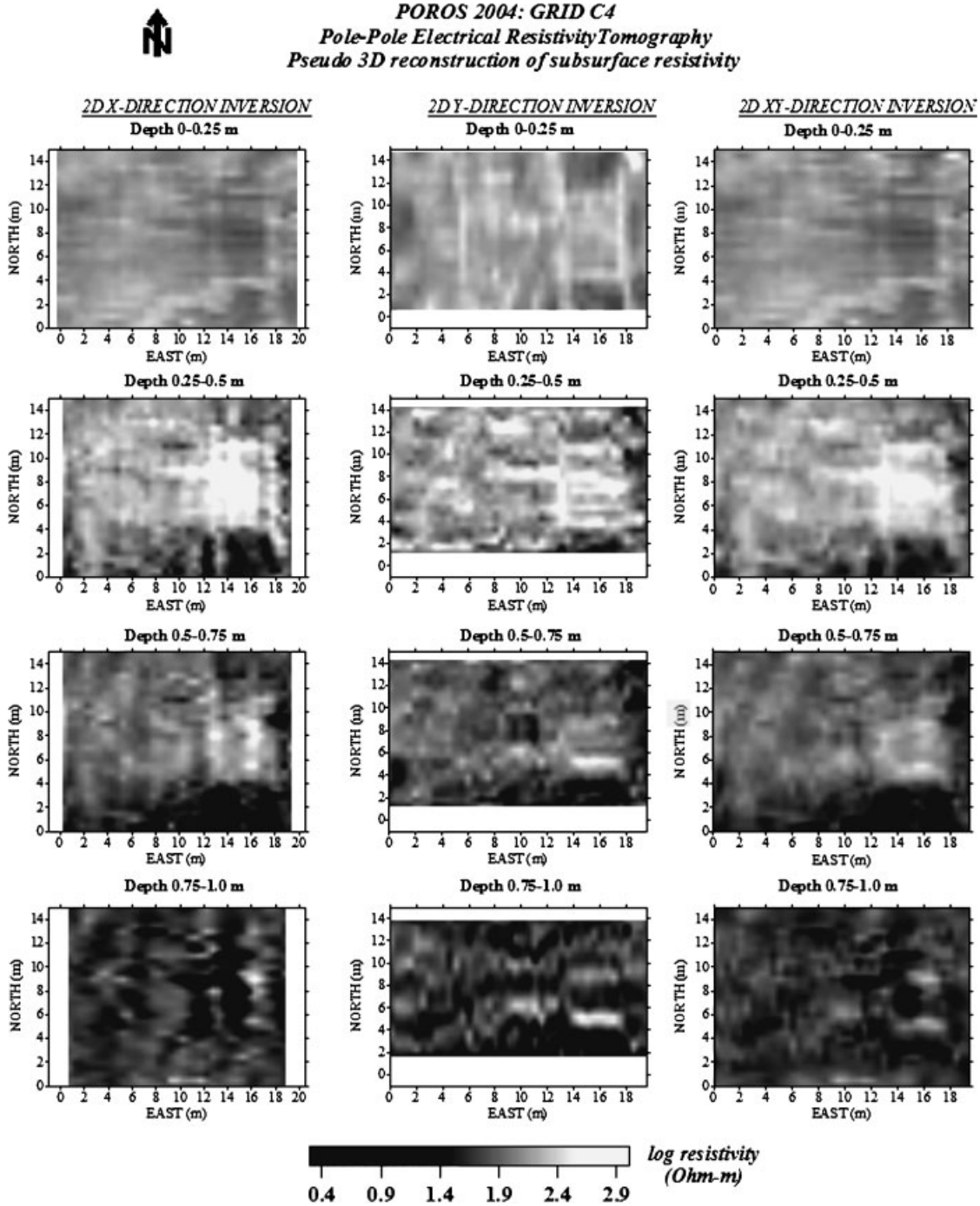

Figure 10. Pesudo three-dimensional representation of the resistivity tomography inversions parallel to the *x* axis (two-dimensional *x* direction inversion), parallel to the *y* axis (two-dimensional *y* direction inversion) and combination of the two directions (two-dimensional *xy* direction inversion). Resistivity values are plotted on a logarithmic scale.

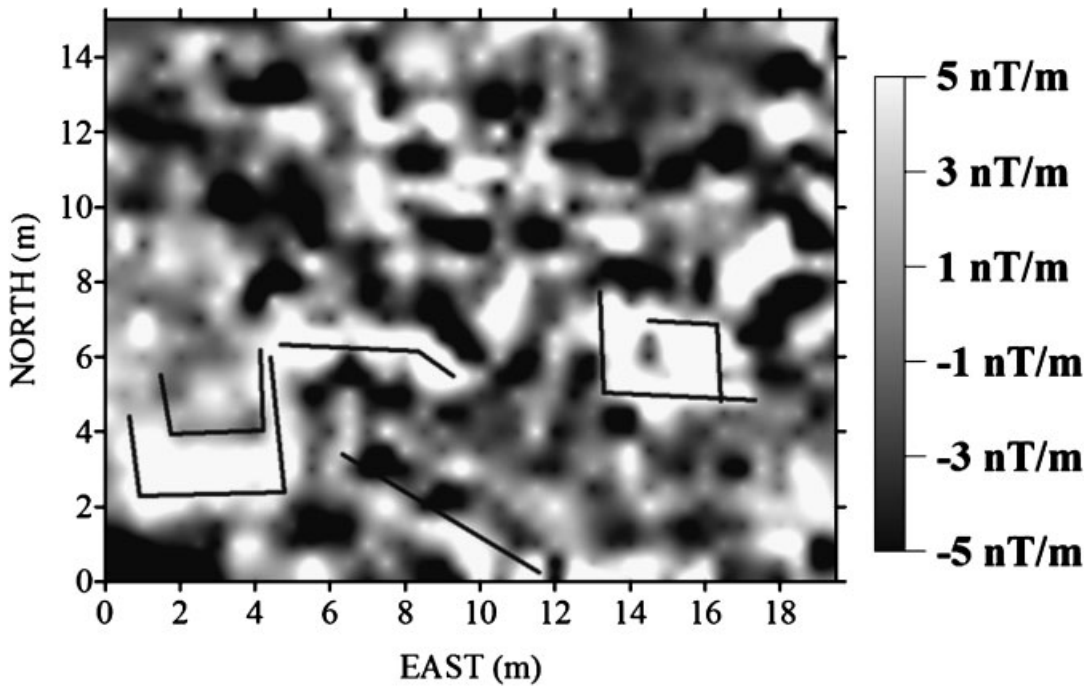

Figure 11. Greyscale image of the magnetic map of grid C4.

Conclusions

Geophysical investigations at the archaeological site of Kalaureia contributed to the enhancement of the archaeological information of the site and in the evaluation of different electrode arrays used in multiplex resistivity surveys. The GPP package that was used in the processing of the magnetic and electrical resistivity data from the archaeological site of Kalaureia proved to be reliable in dealing with datasets of different degrees of noise and quality.

The vertical magnetic gradient surveys in the areas A, B and C1–3 indicated a number of linear and rectangular features, which are probably related to buried archaeological structures. The area southwest of the sanctuary seems to include more relics than the western side of area A. These features extend towards buildings C and D, which represent the later phases of the sanctuary. Evidence for features belonging to different occupation periods of the site is suggested in areas B and C. More particular, most of the rectangular features in area C1–3, along with the linear features in area C4, have a N–S orientation, which is different from the NW–SE orientation of the already excavated structural complexes (buildings A–F).

In general, the magnetic maps were more informative than electrical resistance maps, especially in areas where shallow depth bedrock occurs. In contrast, resistivity data seem to be much more successful in delineating the outline of the features and their internal details towards the southern and southwest part of the surveyed sections. In particular, in area C4, resistivity measurements managed to map the vertical extent of the structural remains up to a depth of about 2 m, but the magnetic data were unable to produce comparative results, mainly due to the increased levels of noise originating from the recent exploitation of the area.

The subsurface resistivity of grid C4 was measured with a four multiplexed twin probe configuration, along with dipole–dipole and Wenner mapping arrays. All three resistivity arrays successfully delineated the outline of the building at the east side of the area, but generally the dipole–dipole configuration was superior compared with the other methods. This is mainly caused by the greater sensitivity of the dipole–dipole configuration in mapping

the horizontal changes of the subsurface resistivity. The twin multiplexed resistivity method provided even further information regarding the depth extent of the archaeological features in the area C4.

A new fieldwork technique, based on the well known RM15–MPX15 resistance meter, was also implemented for the first time, in order to gather parallel tomographic resistivity data in a relatively small amount of time. The data were processed using a two dimensional non-linear inversion algorithm. The resistivity inversion enhanced the outline of the features and was able to resolve a few more details, and it determined the true burial depth and the depth extent of them. The gathering of parallel electrical tomographies, according to the procedure described, and the processing of these data with a two-dimensional inversion algorithm can be used to reconstruct the subsurface resistivity distribution and determine the location, burial depth and depth extent of the buried features.

References

Constable S, Parker R, Constable C. 1987. Occam's inversion: a practical algorithm for generating smooth models from electromagnetic sounding data. *Geophysics* **52**: 289–300.

deGroot-Hedlin C, Constable S. 1990. Occam's inversion to generate smooth, two-dimensional models from magnetotelluric data. *Geophysics* **55**: 1613–1624.

Kalokerinos G, Kokinou E, Sarris A, Vallianatos F. 2004. GPP: a program to automate the geophysical data processing. *First International Conference on Advances in Mineral Resources Management and Environmental Geotechnology, AMIREG 2004*, 7–9 June, Chania, Crete.

McGillivray P, Oldenburg D. 1990. Methods for calculating Frechet derivatives and sensitivities for the non-linear inverse problem: a comparative study. *Geophysical Prospecting* **38**: 499–524.

Sasaki Y. 1989. 2-D joint inversion of magnetotelluric and dipole–dipole resistivity data. *Geophysics* **54**: 254–262.

Sasaki Y. 1992. Resolution of resistivity tomography inferred from numerical simulation. *Geophysical Prospecting* **40**: 453–464.

Tsourlos P. 1995. *Modelling, interpretation and inversion of multielectrode resistivity survey data*. Unpublished PdD thesis, University of York.

Wells B, Penttinen A, Billot M-Fr. 2003. Investigations in the Poseidon Sanctuary on Kalaureia 1997–2001. *Opuscula Atheniensia* **28**: 29–87.

Wells B, Penttinen A, Hjohlman J, Savini E. 2005. The Kalaureia Excavation project: the 2003 season. *Opuscula Atheniensia* **30**: 25–86.

Welter G. 1941. *Troizen und Kalaureia*. Archaäologisches Institut des Deutschen Reiches: Berlin.

Wide S, Kjellberg L. 1895. Ausgrabungen auf Kalaureia. *Athenische Mitteilungen* **20**: 267–326.

